

An efficient numerical method for simulating two-dimensional non-periodic metasurfaces

Fuhao Liu ^{*} ¹ and Ya Yan Lu ^{1,2}

¹Liu Bie Ju Centre for Mathematical Sciences, City University of Hong Kong, Kowloon, Hong Kong, China

²Department of Mathematics, City University of Hong Kong, Kowloon, Hong Kong, China

January 21, 2026

Abstract

Metasurfaces are extremely useful for controlling and manipulating electromagnetic waves. Full-wave numerical simulation is highly desired for their design and optimization, but it is notoriously difficult, even for two-dimensional metasurfaces, when they comprise a huge number of subwavelength elements. This paper focuses on two-dimensional non-periodic metasurfaces that contain only a relatively small number of distinct subwavelength elements. We develop an efficient numerical method based on Neumann-to-Dirichlet operators, the finite element method and local function expansions. Our method drastically reduces the total number of unknowns and is capable of simulating two-dimensional metasurfaces with 10^5 subwavelength elements on a personal computer. Numerical examples demonstrate that the method maintains high accuracy while offering significant advantages in both computational time and memory usage compared to the classical full-domain finite element method, making it particularly suited for the analysis of large metasurfaces.

Keywords: Metasurface; Neumann-to-Dirichlet operator; Finite element method; Helmholtz equation

1 Introduction

Metasurfaces are structures obtained by arranging a huge number of subwavelength dielectric or metallic elements (often called resonators or scatterers) on a substrate or slab [1–3]. They provide exceptional control over electromagnetic waves, allowing precise manipulation of their phase, amplitude, polarization, and wavefront. Due to their compact form and relatively simple fabrication process, metasurfaces have found numerous applications, such as metlenses, beam deflectors, splitters, invisible cloaks, holograms, waveplates, optical mode converters [2–9].

The design of metasurfaces typically follows a multi-step process. Initially, a set of subwavelength elements is designed or selected. These elements are then arranged on a substrate or slab in a predefined pattern. Subsequently, the entire device is numerically simulated to verify its performance. If the metasurface fails to meet the target specifications, the arrangement and simulation steps are iterated as necessary. Numerical simulation plays a critical role in metasurface development, since it is essential for verifying performance and mitigating high manufacturing costs. In principle, full-wave simulation should be used for modeling metasurfaces. Notable examples include the finite-difference time-domain (FDTD) [10, 11] and discontinuous Galerkin time-domain (DGTD) [12, 13] methods, along with the finite-difference method (FDM) [14], finite element method (FEM) [15–18], integral equation method [19] and spectral element method (SEM) [20] in the frequency domain. However, the size of a practical metasurface is usually very large (on the order of 10^4 wavelengths or more), hence these classical methods often require prohibitively large computer memory and extremely long computation time. This makes full-wave simulation of metasurfaces a very challenging problem. To tackle this difficulty, some improved or alternative methods are proposed, such as domain decomposition method [21–27], numerical mode-matching method [28–30], **axisymmetric FEM** [31], integral equations method with fast direct solvers [32] and parallel-accelerated FDTD method [33–35]. Notably, this last method underpins the GPU-accelerated engines in many commercial solvers, such as Ansys Lumerical FDTD, XFDTD, and Tidy3D. Some of these methods are primarily suited for problems with special structures, while others may require many iterations. To avoid the difficulty

^{*}Corresponding author: fuhao.liu@cityu.edu.hk

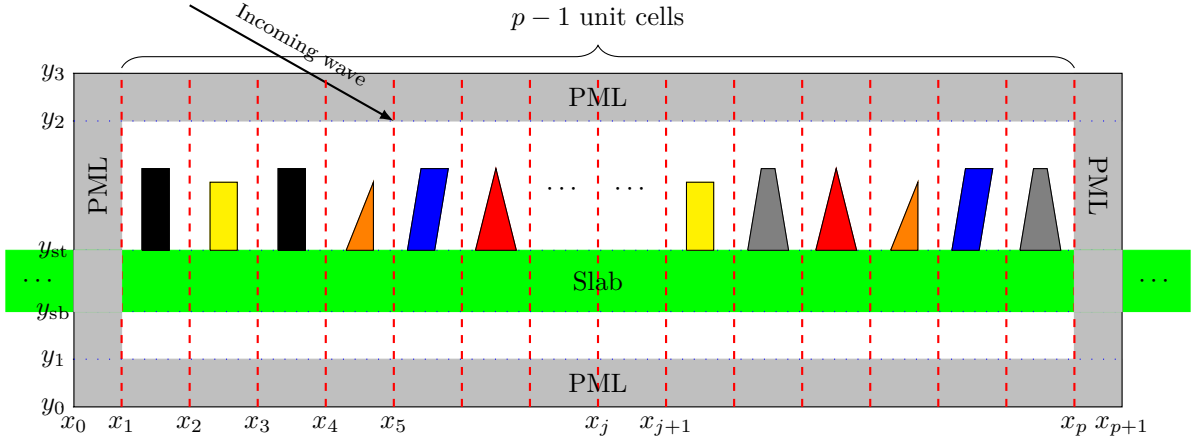


Figure 1: Sketch of a non-periodic 2D metasurface, which can be divided into $p - 1$ unit cells.

of full-wave simulation, some researchers developed local methods, such as the local periodic approximation method [36–38] and the overlapping domain approximation approach [39]. However, these local methods always give rise to relatively large simulation errors.

In this paper, we study two-dimensional (2D) metasurfaces which are translationally invariant in one spatial direction. Full-wave numerical simulation of a large 2D metasurface is still very difficult, when the size of the metasurface is 10^4 wavelengths or more. We focus on non-periodic 2D metasurfaces with a very large number of unit cells (each containing a subwavelength element), assuming that the number of distinct unit cells is relatively small. Notice that a metasurface is an engineered structure based on pre-designed subwavelength elements. The number of distinct subwavelength elements is usually relatively small. Taking advantage of this structural character, we develop an efficient full-wave numerical method based on the concept of Neumann-to-Dirichlet (NtD) operator. For a given domain Ω and a linear homogeneous differential equation, the NtD operator maps the normal derivative of any solution u to u itself on the boundary of Ω . In numerical implementations, the NtD operator is approximated by a matrix. We use FEM to calculate the NtD matrices. To reduce the size of the NtD matrices, we further use local function expansions on the boundary of the domain. In previous works, NtD- or DtN-based methods have been used to solve scattering problems [40] and calculate waveguide modes [41]. A 2D metasurface, although very large in one spatial direction, is still finite in the 2D plane. In our implementation, we surround the metasurface with perfectly matched layers (PMLs), divide the truncated structure into unit cells, and derive a linear system for the normal derivative of the field on the interfaces between the unit cells. Once the linear system is solved, we can easily reconstruct the wave field within every unit cell. Numerical examples confirm that our method is accurate and efficient for simulating large 2D metasurfaces.

The structure of this paper is as follows. Section 2 provides an overview of our method, including the definition of the NtD operators and the derivation of the final linear system. Section 3 details the calculation of a relationship between the fields at two edges of each unit cell and the incident wave. In Sec. 4, local function expansions are combined with FEM to obtain small matrix approximations of the NtD operators. Section 5 describes the procedure for recovering the far field from the near field. In Sec. 6, the accuracy and efficiency of our method are verified by simulating a gradient-phase metasurface, with results compared to those from the classical FEM. We also present a comparison of the computation time and peak memory consumption required by both methods. Finally, Section 7 concludes the paper.

2 Overview of the method

Consider a non-periodic 2D metasurface, which consists of tens of thousands of non-magnetic objects on an infinite dielectric slab in free space. For 2D structures that are invariant in the z -direction, if waves propagate in the x - y plane, the governing equation for the z -component of the electric field u is the Helmholtz equation

$$\nabla \cdot (\nabla u) + k_0^2 n^2 u = 0, \quad (1)$$

where k_0 is the wavenumber in free space, $n = n(x, y)$ is the refractive index function, and $\nabla = (\partial_x, \partial_y)^\top$ is the gradient operator.

As shown in Fig. 1, in the y direction, the metasurface is contained in the interval (y_1, y_2) where the medium

for $y < y_1$ and $y > y_2$ is free space. We assume that the metasurface can be divided into $p - 1$ unit cells, where the j -th unit cell corresponds to $x \in (x_j, x_{j+1})$. For $x < x_1$ and $x > x_p$, the structure is a simple uniform slab with the refractive index n depending on y only, that is

$$n(y) = \begin{cases} n_s > 1, & y_{\text{sb}} < y < y_{\text{st}}, \\ 1, & \text{otherwise,} \end{cases}$$

where $y_1 \leq y_{\text{sb}} < y_{\text{st}} < y_2$. Therefore, the metasurface is contained in the rectangular domain $(x_1, x_p) \times (y_1, y_2)$, where $x_p - x_1$ is significantly larger than $y_2 - y_1$. We consider a scattering problem, where the metasurface is illuminated from above by an incoming wave. The incoming wave is a plane wave given by

$$u^{\text{inc}}(x, y) = \exp(i(\alpha x - \beta y)), \quad \alpha = k_0 \sin(\theta), \quad \beta = k_0 \cos(\theta), \quad (2)$$

where $i = \sqrt{-1}$, and θ is the incident angle.

To truncate the infinite media, we use a perfectly matched layer (PML) to surround the rectangular domain $(x_1, x_p) \times (y_1, y_2)$. The PML corresponds to the intervals (x_0, x_1) , (x_p, x_{p+1}) , (y_0, y_1) and (y_2, y_3) . Therefore, the entire computational domain is the rectangle $(x_0, x_{p+1}) \times (y_0, y_3)$. For the incident wave given in Eq. (2), if there are no objects on the slab, we can easily find the reflected and transmitted waves. The exact solution u^{ref} is:

$$u^{\text{ref}} = \begin{cases} \exp(i[\alpha x - \beta(y - y_{\text{st}})]) + C_0 \exp(i[\alpha x + \beta(y - y_{\text{st}})]), & y \geq y_{\text{st}}, \\ C_1 \exp(i[\alpha x - \beta_s(y - y_{\text{st}})]) + C_2 \exp(i[\alpha x + \beta_s(y - y_{\text{sb}})]), & y_{\text{sb}} < y < y_{\text{st}}, \\ C_3 \exp(i[\alpha x - \beta(y - y_{\text{sb}})]), & y \leq y_{\text{sb}}, \end{cases} \quad (3)$$

where $\beta_s = \sqrt{(k_0 n_s)^2 - \alpha^2}$, and the coefficients C_0, C_1, C_2, C_3 satisfy a system of equations obtained from the continuity of u^{ref} and $\partial_y u^{\text{ref}}$ at $y = y_{\text{sb}}$ and $y = y_{\text{st}}$.

Since the PML is used to simulate outgoing waves and the total wave u^{tot} (containing the incident wave) is not outgoing, we need to subtract u^{ref} from the total wave in the PML region. To simplify the notation, we let

$$u = \begin{cases} u^{\text{tot}} - u^{\text{ref}}, & \text{in PML,} \\ u^{\text{tot}}, & \text{in } (x_1, x_p) \times (y_1, y_2). \end{cases} \quad (4)$$

The entire computational domain $(x_0, x_{p+1}) \times (y_0, y_3)$ can be divided into $p + 1$ subdomains

$$\Omega_j = \{(x, y) | x_j < x < x_{j+1}, y_0 < y < y_3\}, \quad j = 0, 1, 2, \dots, p,$$

where Ω_0 and Ω_p are the left and right PML regions. The interfaces between the subdomains are

$$\Gamma_j = \{(x, y) | x = x_j, y_0 < y < y_3\}, \quad j = 1, 2, \dots, p.$$

Our method involves two steps. In the first step, we calculate an operator $\Lambda^{(j)}$ and a function $f^{(j)}$ for each unit cell Ω_j . In the second step, we set up a block tridiagonal linear system for $\partial_x u$ at all Γ_j . Here, $\Lambda^{(j)}$ ($1 \leq j \leq p - 1$) is the NtD operator of Ω_j , which maps $\partial_x u$ at Γ_j and Γ_{j+1} to u at Γ_j and Γ_{j+1} . The function $f^{(j)}$ accounts for the incident wave. The relationship between u and $\partial_x u$ at Γ_j and Γ_{j+1} will be

$$\begin{bmatrix} u_j \\ u_{j+1} \end{bmatrix} = \Lambda^{(j)} \begin{bmatrix} \partial_x u_j \\ \partial_x u_{j+1} \end{bmatrix} + f^{(j)}, \quad \Lambda^{(j)} = \begin{bmatrix} \Lambda_{11}^{(j)} & \Lambda_{12}^{(j)} \\ \Lambda_{21}^{(j)} & \Lambda_{22}^{(j)} \end{bmatrix}, \quad f^{(j)} = \begin{bmatrix} f_1^{(j)} \\ f_2^{(j)} \end{bmatrix}, \quad j = 1, 2, \dots, p - 1, \quad (5)$$

where u_j , u_{j+1} , $\partial_x u_j$, $\partial_x u_{j+1}$ denote u and $\partial_x u$ on Γ_j and Γ_{j+1} , respectively. For the left and right PML regions, the relationships are

$$u_1 = \Lambda^{(0)} \partial_x u_1 + f^{(0)}, \quad u_p = \Lambda^{(p)} \partial_x u_p + f^{(p)}. \quad (6)$$

Evaluating u_{j+1} ($1 \leq j \leq p - 2$) from Eq. (5) and a similar equation for Ω_{j+1} , we obtain

$$\Lambda_{21}^{(j)} \partial_x u_j + (\Lambda_{22}^{(j)} - \Lambda_{11}^{(j+1)}) \partial_x u_{j+1} - \Lambda_{12}^{(j+1)} \partial_x u_{j+2} = f_1^{(j+1)} - f_2^{(j)}, \quad (7)$$

Similarly, by evaluating u_1 and u_p from Eq. (6), we obtain

$$\begin{aligned} (\Lambda^{(0)} - \Lambda_{11}^{(1)})\partial_x u_1 - \Lambda_{12}^{(1)}\partial_x u_2 &= f_1^{(1)} - f^{(0)}, \\ \Lambda_{21}^{(p-1)}\partial_x u_{p-1} + (\Lambda_{22}^{(p-1)} - \Lambda^{(p)})\partial_x u_p &= f^{(p)} - f_2^{(p-1)}. \end{aligned} \quad (8)$$

Equations (8) and (7) for $j = 1, 2, \dots, p-2$ can be rewritten as the following block tridiagonal linear system

$$\begin{bmatrix} \Pi_1 & -\Lambda_{12}^{(1)} & & & \\ \Lambda_{21}^{(1)} & \Pi_2 & -\Lambda_{12}^{(2)} & & \\ & \ddots & \ddots & \ddots & \\ & & \Lambda_{21}^{(p-2)} & \Pi_{p-1} & -\Lambda_{12}^{(p-1)} \\ & & & \Lambda_{21}^{(p-1)} & \Pi_p \end{bmatrix} \begin{bmatrix} \partial_x u_1 \\ \partial_x u_2 \\ \vdots \\ \partial_x u_{p-1} \\ \partial_x u_p \end{bmatrix} = \begin{bmatrix} f_1^{(1)} - f^{(0)} \\ f_1^{(2)} - f_2^{(1)} \\ \vdots \\ f_1^{(p-1)} - f_2^{(p-2)} \\ f^{(p)} - f_2^{(p-1)} \end{bmatrix}, \quad (9)$$

where $\Pi_1 = \Lambda^{(0)} - \Lambda_{11}^{(1)}$, $\Pi_p = \Lambda_{22}^{(p-1)} - \Lambda^{(p)}$, $\Pi_j = \Lambda_{22}^{(j-1)} - \Lambda_{11}^{(j)}$, $j = 1, 2, \dots, p-1$.

Each $\Lambda^{(j)}$ in this section can be approximated by a small matrix, and each $f^{(j)}$ can be approximated by a column vector. Since those $\Lambda^{(j)}$ for identical unit cells are the same, they require computation only once and are parallelizable. Although all $f^{(j)}$ are different, they can be calculated efficiently and in parallel. In this paper, we assume that there are only p_0 distinct unit cells. Therefore, if $p_0 \ll p$, our method is efficient.

3 Boundary relationships for unit cells

In this section, we discuss the calculation of $\Lambda^{(j)}$ and $f^{(j)}$ in Eqs. (5) and (6). According to Eq. (4), we know that u is discontinuous on the interface between the PML region and the rectangle $(x_1, x_p) \times (y_1, y_2)$. Therefore, as shown in Fig. 2(b), domain Ω_j ($1 \leq j \leq p-1$) needs to be divided into three subdomains

$$\Omega_j^{(k)} = \{(x, y) | x_j < x < x_{j+1}, y_k < y < y_{k+1}\}, \quad k = 0, 1, 2.$$

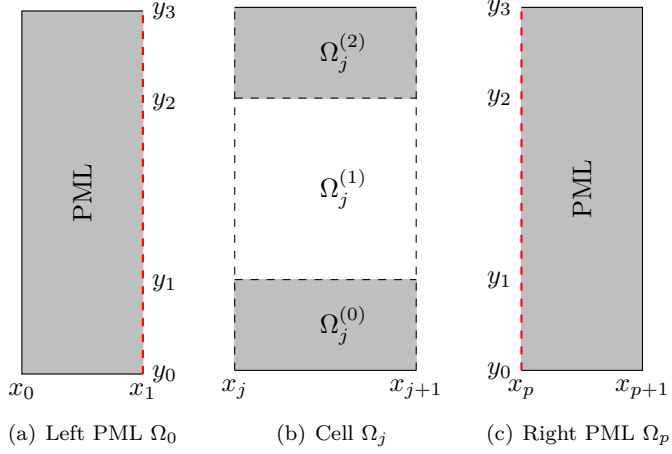


Figure 2: The sketches of the j -th cell and the left and right PML.

Since the PML transforms outgoing waves into exponentially decaying solutions, we can assume $u = 0$ at the exterior boundary of the PML region. Within each subdomain $\Omega_j^{(k)}$, u satisfies the following equation:

$$\nabla \cdot (S \nabla u) + k_0^2 n^2 s_x s_y u = 0, \quad (10)$$

where S , s_x and s_y are

$$S = \begin{bmatrix} s_y/s_x & \\ & s_x/s_y \end{bmatrix}, \quad s_x(x) = 1 + i\sigma_x(x), \quad s_y(y) = 1 + i\sigma_y(y). \quad (11)$$

In Eq. (11), σ_x and σ_y are real functions given as

$$\sigma_x(x) = \begin{cases} b \frac{(x_1 - x)^4}{(x_1 - x_0)^4}, & x_0 \leq x \leq x_1, \\ b \frac{(x - x_p)^4}{(x_{p+1} - x_p)^4}, & x_p \leq x \leq x_{p+1}, \\ 0, & \text{otherwise,} \end{cases} \quad \sigma_y(y) = \begin{cases} b \frac{(y_1 - y)^4}{(y_1 - y_0)^4}, & y_0 \leq y \leq y_1, \\ b \frac{(y - y_2)^4}{(y_3 - y_2)^4}, & y_2 \leq y \leq y_3, \\ 0, & \text{otherwise,} \end{cases}$$

where b denotes a positive constant [42–44].

To obtain Eq. (5), we first calculate the NtD operator $\Lambda^{(j,k)}$ for each subdomain $\Omega_j^{(k)}$ (with $k = 0, 1, 2$). To simplify notation, we let

$$u_j^{(k)} = u(x_j, y), \quad \partial_x u_j^{(k)} = \partial_x u(x_j, y), \quad y \in (y_k, y_{k+1}), \quad j = 1, 2, \dots, p, \quad k = 0, 1, 2.$$

Notice that for all j , $u_j^{(1)}$ and $\partial_x u_j^{(1)}$ represent the total solution that contains u^{ref} . In addition, we define

$$w_j^{(k,\pm)} = u(x, y_k^\pm), \quad \partial_y w_j^{(k,\pm)} = \partial_y u(x, y_k^\pm), \quad w_j^{(\text{ref},k)} = u^{\text{ref}}(x, y_k), \quad \partial_y w_j^{(\text{ref},k)} = \partial_y u^{\text{ref}}(x, y_k),$$

where $x \in (x_j, x_{j+1})$, $j = 1, 2, \dots, p-1$, $k = 1, 2$. Here, $u(x, y_k^\pm)$ represents the limit as u approaches $y = y_k$ from below or above.

To construct the NtD operator $\Lambda^{(j,1)}$ ($1 \leq j \leq p-1$), we need to order the four edges of $\Omega_j^{(1)}$. If the four edges are ordered as “bottom, left, right, and top”, then $\Lambda^{(j,1)}$ satisfies

$$\Lambda^{(j,1)} \begin{bmatrix} \partial_y w_j^{(1,+)} \\ \partial_x u_j^{(1)} \\ \partial_x u_{j+1}^{(1)} \\ \partial_y w_j^{(2,-)} \end{bmatrix} = \begin{bmatrix} \Lambda_{11}^{(j,1)} & \Lambda_{12}^{(j,1)} & \Lambda_{13}^{(j,1)} & \Lambda_{14}^{(j,1)} \\ \Lambda_{21}^{(j,1)} & \Lambda_{22}^{(j,1)} & \Lambda_{23}^{(j,1)} & \Lambda_{24}^{(j,1)} \\ \Lambda_{31}^{(j,1)} & \Lambda_{32}^{(j,1)} & \Lambda_{33}^{(j,1)} & \Lambda_{34}^{(j,1)} \\ \Lambda_{41}^{(j,1)} & \Lambda_{42}^{(j,1)} & \Lambda_{43}^{(j,1)} & \Lambda_{44}^{(j,1)} \end{bmatrix} \begin{bmatrix} \partial_y w_j^{(1,+)} \\ \partial_x u_j^{(1)} \\ \partial_x u_{j+1}^{(1)} \\ \partial_y w_j^{(2,-)} \end{bmatrix} = \begin{bmatrix} w_j^{(1,+)} \\ u_j^{(1)} \\ u_{j+1}^{(1)} \\ w_j^{(2,-)} \end{bmatrix}. \quad (12)$$

For $\Omega_j^{(0)}$ and $\Omega_j^{(2)}$, the corresponding NtD operators are defined on only three edges where u is unknown. For $\Lambda^{(j,0)}$, the three edges are ordered as “left, right, and top”. Similarly, the three edges of $\Omega_j^{(2)}$ are ordered as “bottom, left and right”. Therefore, $\Lambda^{(j,0)}$ and $\Lambda^{(j,2)}$ are 3×3 matrix operators satisfying

$$\Lambda^{(j,0)} \begin{bmatrix} \partial_x u_j^{(0)} \\ \partial_x u_{j+1}^{(0)} \\ \partial_y w_j^{(1,-)} \end{bmatrix} = \begin{bmatrix} u_j^{(0)} \\ u_{j+1}^{(0)} \\ w_j^{(1,-)} \end{bmatrix}, \quad \Lambda^{(j,2)} \begin{bmatrix} \partial_y w_j^{(2,+)} \\ \partial_x u_j^{(2)} \\ \partial_x u_{j+1}^{(2)} \end{bmatrix} = \begin{bmatrix} w_j^{(2,+)} \\ u_j^{(2)} \\ u_{j+1}^{(2)} \end{bmatrix}. \quad (13)$$

To construct the NtD operators for Ω_0 and Ω_p , there is no need to divide Ω_0 and Ω_p to subdomains. However, the field u is discontinuous across the lines $x = x_1$ and $x = x_p$ within the vertical interval $y_1 < y < y_2$. This is because $u = u^{\text{tot}}$ for $x_1 < x < x_p$, but $u = u^{\text{tot}} - u^{\text{ref}}$ for $x < x_1$ and $x > x_p$. In addition, $u = 0$ on the three exterior edges of Ω_0 and Ω_p . Therefore, $\Lambda^{(0)}$ and $\Lambda^{(p)}$ are 3×3 matrix operators satisfying

$$\Lambda^{(0)} \begin{bmatrix} \partial_x u_1^{(0)} \\ \partial_x u_1^{(1)} - \partial_x u_1^{(\text{ref},1)} \\ \partial_x u_1^{(2)} \end{bmatrix} = \begin{bmatrix} u_1^{(0)} \\ u_1^{(1)} - u_1^{(1)} \\ u_1^{(2)} \end{bmatrix}, \quad \Lambda^{(p)} \begin{bmatrix} \partial_x u_p^{(0)} \\ \partial_x u_p^{(1)} - \partial_x u_p^{(\text{ref},1)} \\ \partial_x u_p^{(2)} \end{bmatrix} = \begin{bmatrix} u_p^{(0)} \\ u_p^{(1)} - u_p^{(1)} \\ u_p^{(2)} \end{bmatrix}, \quad (14)$$

where $u_1^{(1)} = u(x_1^+, y)$, $\partial_x u_1^{(1)} = \partial_x u(x_1^+, y)$, $u_j^{(1)} = u^{\text{ref}}(x_1, y)$, $\partial_x u_j^{(\text{ref},1)} = \partial_x u^{\text{ref}}(x_j, y)$ for $y_1 < y < y_2$. Similarly, $u_p^{(1)}$ and other quantities with subscript p are obtained at $x = x_p^-$. From Eqs. (14), we easily obtain

$$f^{(0)} = \begin{bmatrix} 0 \\ u_1^{(1)} \\ 0 \end{bmatrix} - \Lambda^{(0)} \begin{bmatrix} 0 \\ \partial_x u_1^{(\text{ref},1)} \\ 0 \end{bmatrix}, \quad f^{(p)} = \begin{bmatrix} 0 \\ u_p^{(1)} \\ 0 \end{bmatrix} - \Lambda^{(p)} \begin{bmatrix} 0 \\ \partial_x u_p^{(\text{ref},1)} \\ 0 \end{bmatrix}. \quad (15)$$

As defined in Eq. (4), we know that u is discontinuous at the interface between the PML region and the

rectangle $(x_1, x_p) \times (y_1, y_2)$, where its jump is given by u^{ref} . Therefore,

$$\begin{aligned} w_j^{(1,-)} &= w_j^{(1,+)} - w_j^{(\text{ref},1)}, \quad \partial_y w_j^{(1,-)} = \partial_y w_j^{(1,+)} - \partial_y w_j^{(\text{ref},1)}, \\ w_j^{(2,+)} &= w_j^{(2,-)} - w_j^{(\text{ref},2)}, \quad \partial_y w_j^{(2,+)} = \partial_y w_j^{(2,-)} - \partial_y w_j^{(\text{ref},2)}, \end{aligned} \quad (16)$$

where $j = 1, 2, \dots, p-1$.

Using the above equations, we can construct $\Lambda^{(j)}$ and $f^{(j)}$. This process involves two steps. First, we evaluate $w_j^{(2,-)}$ and $w_j^{(1,+)}$ from Eqs. (12) and (13), and substitute into Eqs. (16). Second, we solve $\partial_y w_j^{(2,-)}$ and $\partial_y w_j^{(1,+)}$, substitute into Eqs. (12) and (13). This leads to a linear relation between u_j , u_{j+1} , their x -derivatives, that is Eq. (5). The inhomogeneous term $f^{(j)}$ is related to u^{ref} . Complete details are provided in Appendix A.

4 Matrix approximation for NtD operators

Since the entries of the coefficient matrix of Eq. (9) are operators, and the elements of the unknown and right-hand-side vectors are functions of y , they must be approximated by matrices and vectors, respectively. There are two approaches to accomplish this. The classical approach is to discretize y by K points, approximate each function of y by a column vector of length K , and approximate each operator by a $K \times K$ matrix. Typically, this approach gives rise to a relatively large K , so that it is relatively expensive to solve Eq. (9). An alternative approach is to approximate each function of y by a sum of properly chosen basis functions, and replace Eq. (9) by a new equation for the expansion coefficients, where the operators in Eq. (9) become matrices relating the coefficients. By taking advantage of the piecewise smoothness of the wave field, the new equation can be much smaller, leading to a more efficient numerical method.

We adopt the second approach, and approximate each function of y the intervals (y_0, y_1) , (y_1, y_2) and (y_2, y_3) separately. Specifically, for the interval (y_2, y_3) , we use the following basis functions:

$$\varphi_{2,m}(y) = (1-t) \exp(-C_2^\varphi t^2) L_{m-1}(2t-1), \quad t = (y-y_2)/(y_3-y_2), \quad m = 1, 2, \dots, N_2,$$

where L_{m-1} is the Legendre polynomial of degree $m-1$, C_2^φ is a positive constant, and N_2 is the total number of basis functions. For the interval (y_0, y_1) , the basis functions are

$$\varphi_{0,m}(y) = (1-t) \exp(-C_0^\varphi t^2) L_{m-1}(2t-1), \quad t = (y-y_1)/(y_0-y_1), \quad m = 1, 2, \dots, N_0.$$

For the interval (y_1, y_2) , we use scaled Legendre polynomials that map (y_1, y_2) to $(-1, 1)$, denote them as $\varphi_{1,m}(y)$, for $m = 1, 2, \dots, N_1$, where each polynomial has degree $m-1$. The total number of basis functions is $N = N_0 + N_1 + N_2$. Therefore, each function of y is associated with N expansion coefficients.

To approximate the operators in Eq. (9), we require the matrix approximations $\tilde{\Lambda}^{(j,k)}$ for the NtD operator $\Lambda^{(j,k)}$, where $k = 0, 1, 2$. The operator $\Lambda^{(j,k)}$ maps the normal derivative of u to u itself on the boundary of $\Omega_j^{(k)}$; correspondingly, the matrix $\tilde{\Lambda}^{(j,k)}$ maps their respective vectors of expansion coefficients. In what follows, we adopt the convention that a tilde over a function denotes the column vector of its expansion coefficients, and a tilde over an operator denotes the matrix that acts on these coefficient vectors. The specific definitions of these vectors are provided in Appendix B.

On the interval (x_j, x_{j+1}) , we approximate each function of x by a sum of M_j scaled Legendre polynomials $\phi_{j,m}(x)$, $m = 1, 2, \dots, M_j$, where each polynomial $\phi_{j,m}(x)$ maps (x_j, x_{j+1}) to $(-1, 1)$. Consequently, matrix $\tilde{\Lambda}^{(j,0)}$ is of dimension $(2N_0 + M_j) \times (2N_0 + M_j)$, $\tilde{\Lambda}^{(j,2)}$ is $(2N_2 + M_j) \times (2N_2 + M_j)$, $\tilde{\Lambda}^{(j,1)}$ is $(2M_j + 2N_1) \times (2M_j + 2N_1)$, and these matrices satisfy

$$\tilde{\Lambda}^{(j,0)} \begin{bmatrix} \partial_x \tilde{u}_j^{(0)} \\ \partial_x \tilde{u}_{j+1}^{(0)} \\ \partial_y \tilde{w}_j^{(1,-)} \end{bmatrix} = \begin{bmatrix} \tilde{u}_j^{(0)} \\ \tilde{u}_{j+1}^{(0)} \\ \tilde{w}_j^{(1,-)} \end{bmatrix}, \quad \tilde{\Lambda}^{(j,1)} \begin{bmatrix} \partial_y \tilde{w}_j^{(1,+)} \\ \partial_x \tilde{u}_j^{(1)} \\ \partial_x \tilde{u}_{j+1}^{(1)} \\ \partial_y \tilde{w}_j^{(2,-)} \end{bmatrix} = \begin{bmatrix} \tilde{w}_j^{(1,+)} \\ \tilde{u}_j^{(1)} \\ \tilde{u}_{j+1}^{(1)} \\ \tilde{w}_j^{(2,-)} \end{bmatrix}, \quad \tilde{\Lambda}^{(j,2)} \begin{bmatrix} \partial_y \tilde{w}_j^{(2,+)} \\ \partial_x \tilde{u}_j^{(2)} \\ \partial_x \tilde{u}_{j+1}^{(2)} \\ \partial_y \tilde{w}_j^{(2,-)} \end{bmatrix} = \begin{bmatrix} \tilde{w}_j^{(2,+)} \\ \tilde{u}_j^{(2)} \\ \tilde{u}_{j+1}^{(2)} \\ \tilde{w}_j^{(2,-)} \end{bmatrix}. \quad (17)$$

In addition, the matrices $\tilde{\Lambda}^{(j,k)}$ ($k = 0, 1, 2$) can be partitioned into blocks, they are given by $\tilde{\Lambda}^{(j,0)} = [\tilde{\Lambda}_{m,l}^{(j,0)}]_{3 \times 3}$, $\tilde{\Lambda}^{(j,1)} = [\tilde{\Lambda}_{m,l}^{(j,1)}]_{4 \times 4}$, $\tilde{\Lambda}^{(j,2)} = [\tilde{\Lambda}_{m,l}^{(j,2)}]_{3 \times 3}$, where $\tilde{\Lambda}_{m,l}^{(j,k)}$ is the (m, l) th block of $\tilde{\Lambda}^{(j,k)}$.

For the NtD operators $\Lambda^{(0)}$ and $\Lambda^{(p)}$, the approximations for $u_j^{(k)}$ and $\partial_x u_j^{(k)}$ ($j = 1, p$, $0 \leq k \leq 2$) follow

the procedure outlined above. Additionally, we need the functions $u_j^{(1)}$ and $\partial_x u_j^{(\text{ref},1)}$ ($j = 1, p$) on the interval (y_1, y_2) , which are also approximated by sums of N_1 scaled Legendre polynomials $\varphi_{1,m}(y)$. Consequently, $\tilde{\Lambda}^{(0)}$, $\tilde{\Lambda}^{(p)}$ are $N \times N$ matrices that satisfy

$$\tilde{\Lambda}^{(0)} \begin{bmatrix} \partial_x \tilde{u}_1^{(0)} \\ \partial_x \tilde{u}_1^{(1)} - \partial_x \tilde{u}_1^{(\text{ref},1)} \\ \partial_x \tilde{u}_1^{(2)} \end{bmatrix} = \begin{bmatrix} \tilde{u}_1^{(0)} \\ \tilde{u}_1^{(1)} - \tilde{u}_1^{(\text{ref},1)} \\ \tilde{u}_1^{(2)} \end{bmatrix}, \quad \tilde{\Lambda}^{(p)} \begin{bmatrix} \partial_x \tilde{u}_p^{(0)} \\ \partial_x \tilde{u}_p^{(1)} - \partial_x \tilde{u}_p^{(\text{ref},1)} \\ \partial_x \tilde{u}_p^{(2)} \end{bmatrix} = \begin{bmatrix} \tilde{u}_p^{(0)} \\ \tilde{u}_p^{(1)} - \tilde{u}_p^{(\text{ref},1)} \\ \tilde{u}_p^{(2)} \end{bmatrix}. \quad (18)$$

Moreover, $\tilde{\Lambda}^{(0)}$ and $\tilde{\Lambda}^{(p)}$ admit a 3×3 block structure, with their (m, l) -th block denoted by $\tilde{\Lambda}_{m,l}^{(j)}$ (for $j = 0, p$ and $1 \leq m, l \leq 3$).

We first discuss the steps for calculating the NtD matrix $\tilde{\Lambda}^{(j,1)}$. According to the approximations for functions $\partial_y w_j^{(1,+)}$, $\partial_y w_j^{(2,-)}$, $\partial_x u_j^{(1)}$ and $\partial_x u_{j+1}^{(1)}$ (see Eqs. (30) and (33) in Appendix B), we need to solve $2(M_j + N_1)$ boundary value problems (BVPs) in subdomain $\Omega_j^{(1)}$. These BVPs are given by the Helmholtz equation (1) with different Neumann boundary conditions (NBCs). For each BVP, the NBC is inhomogeneous on one edge and is zero on all other edges. More precisely, the inhomogeneous NBC specifies that the x or y derivative of the solution equals $\varphi_{1,m}(y)$ or $\phi_{j,m}(x)$, respectively. Those BVPs are ordered by edge “bottom, left, right, top” and then by basis function index ($m = 1, 2, \dots, N_1$ or M_j). We use FEM to solve these BVPs. The corresponding linear systems have the same coefficient matrix and different right-hand side vectors. Therefore, these linear systems can be solved together efficiently. Let v be the solution of a particular BVP. We expand the trace of v on the four edges as

$$\begin{aligned} v(x, y_1) &\approx \sum_{m=1}^{M_j} \tilde{v}_m^{(1)} \phi_{j,m}(x), & v(x, y_2) &\approx \sum_{m=1}^{M_j} \tilde{v}_m^{(4)} \phi_{j,m}(x), & x \in (x_j, x_{j+1}), \\ v(x_j, y) &\approx \sum_{m=1}^{N_1} \tilde{v}_m^{(2)} \varphi_{1,m}(y), & v(x_{j+1}, y) &\approx \sum_{m=1}^{N_1} \tilde{v}_m^{(3)} \varphi_{1,m}(y), & y \in (y_1, y_2). \end{aligned}$$

The coefficients are arranged into a column vector as follows:

$$\left[\tilde{v}_1^{(1)}, \dots, \tilde{v}_{M_j}^{(1)}, \tilde{v}_1^{(2)}, \dots, \tilde{v}_{N_1}^{(2)}, \tilde{v}_1^{(3)}, \dots, \tilde{v}_{N_1}^{(3)}, \tilde{v}_1^{(4)}, \dots, \tilde{v}_{M_j}^{(4)} \right]^\top.$$

This vector itself forms a column of the matrix $\tilde{\Lambda}^{(j,1)}$, ordered according to the sequence prescribed to the BVPs.

Next, we describe the steps for calculating the matrix $\tilde{\Lambda}^{(j,0)}$. The two functions $\partial_x u_j^{(0)}$ and $\partial_x u_{j+1}^{(0)}$ are approximated by sums of N_0 basis functions $\varphi_{0,m}(y)$, and $\partial_y w_j^{(1,-)}$ is approximated by a sum of M_j scaled Legendre polynomials $\phi_{j,m}(x)$. Similar to the matrix $\tilde{\Lambda}^{(j,1)}$, we need to solve $(2N_0 + M_j)$ BVPs in $\Omega_j^{(0)}$. These BVPs are given by Eq. (10) with homogeneous Dirichlet boundary condition imposed on the bottom edge and different NBCs imposed on all other edges. For each BVP, the NBC is nonzero on one edge and is zero on other two edges. More precisely, the nonzero NBC specifies that the x or y derivative of the solution equals $\varphi_{0,m}(y)$ or $\phi_{j,m}(x)$, respectively. All these BVPs are ordered first by edge “left, right, top”, then for each edge by the basis functions $m = 1, 2, \dots, N_0$ or M_j . Same as before, we expand the solutions of these BVPs at the three edges (left, right, top), and the corresponding expansion coefficients give rise to the entries of the matrix $\tilde{\Lambda}^{(j,0)}$. The matrix $\tilde{\Lambda}^{(j,2)}$ can be calculated by the same method, with the corresponding BVPs ordered by edge “bottom, left, right”.

Finally, we describe the steps for calculating the matrix $\tilde{\Lambda}^{(0)}$. The three functions $\partial_x u_1^{(k)}$ ($0 \leq k \leq 2$) are approximated by sums of N_k functions $\varphi_{k,m}(y)$, respectively, and $\partial_x u_1^{(\text{ref},1)}$ is approximated by a sum of N_1 scaled Legendre polynomials $\varphi_{1,m}(y)$. Therefore, similar to the procedure outlined above, we need to solve N BVPs in Ω_0 . These BVPs are given by Eq. (10) with different NBCs imposed on the right edge and homogeneous Dirichlet boundary condition imposed on all other edges. These NBCs are also piecewisely defined. For each BVP, the x derivative of the solution on sub-interval (y_k, y_{k+1}) of the right edge equals $\varphi_{k,1}(y)$ and is zero on the remaining parts. For each BVP, the solution on the interval (y_k, y_{k+1}) can be expanded in the same way as $\partial_x u_1^{(k)}$, where $k = 0, 1, 2$. The expansion coefficients form a column of matrix $\tilde{\Lambda}^{(0)}$. The NtD matrix $\tilde{\Lambda}^{(p)}$ can be calculated similarly.

Using the NtD matrices for the subdomains $\Omega_j^{(k)}$, $k = 0, 1, 2$, and following the procedure given in Sec. 3, we compute the matrix $\tilde{\Lambda}^{(j)}$ and the source vector $\tilde{f}^{(j)}$ for $f^{(j)}$. For this step, the continuity conditions at $y = y_1$

and $y = y_2$ are given as

$$\begin{aligned}\tilde{w}_j^{(1,-)} &= \tilde{w}_j^{(1,+)} - \tilde{w}_j^{(\text{ref},1)}, & \partial_y \tilde{w}_j^{(1,-)} &= \partial_y \tilde{w}_j^{(1,+)} - \partial_y \tilde{w}_j^{(\text{ref},1)}, \\ \tilde{w}_j^{(2,+)} &= \tilde{w}_j^{(2,-)} - \tilde{w}_j^{(\text{ref},2)}, & \partial_y \tilde{w}_j^{(2,+)} &= \partial_y \tilde{w}_j^{(2,-)} - \partial_y \tilde{w}_j^{(\text{ref},2)},\end{aligned}\quad (19)$$

where $\tilde{w}_j^{(\text{ref},k)}$ ($k = 1, 2$) are the expansion coefficients of $w_j^{(\text{ref},k)}$.

By following the discretization procedure for Eq. (9), we obtain a block tridiagonal matrix linear system that we denote as (9A), which has the same form as Eq. (9) with every quantity (entries of the coefficient matrix and the elements of the unknown and right-hand-side vectors) replaced by its tilde-adorned discrete counterpart. Equation (9A) can be solved using block LU factorization [45], the complexity of which is $O(N^3p)$. Its solution yields $\partial_y \tilde{w}_j^{(1,+)}$ and $\partial_y \tilde{w}_j^{(2,-)}$ following the procedure given in Appendix A. Then, we use Eq. (19) to obtain $\partial_y \tilde{w}_j^{(1,-)}$ and $\partial_y \tilde{w}_j^{(2,+)}$. Finally, the wave field in each subdomain is reconstructed as a linear combination of the BVP solutions used to build the local NtD matrix, with the combination weights directly provided by the solution of system (9A).

5 Far-field by plane wave expansion

Using the method described in the previous section, we obtain the wave field within a bounded domain $(x_1, x_p) \times (y_1, y_2)$. However, the far-field is often of primary interest. To recover the far-field for $y > y_2$ and $y < y_1$, we first recover the data on the lines $y = y_1$ and $y = y_2$ for $x < x_1$ and $x > x_p$ using data from the PML region, then compute the Fourier transform of this data along lines $y = y_1$ and y_2 , and finally apply the inverse Fourier transform to recover the far-field.

For $y > y_2$, the scattering field $u^{(\text{s})} = u^{\text{tot}} - u^{\text{ref}}$ satisfies Eq. (1) for refractive index $n = 1$. Applying the Fourier transform to Eq. (1) with respect to x , we obtain

$$\frac{\partial^2 \hat{u}^{(\text{s})}(\alpha, y)}{\partial y^2} + \beta^2 \hat{u}^{(\text{s})}(\alpha, y) = 0, \quad \beta = \beta(\alpha) = \sqrt{k_0^2 - \alpha^2}. \quad (20)$$

The Fourier transform of $u^{(\text{s})}(x, y_2)$ is

$$\hat{u}^{(\text{s})}(\alpha, y_2) = \int_{-\infty}^{\infty} u^{(\text{s})}(x, y_2) \exp(-i\alpha x) dx = \left(\int_{-\infty}^{x_1} + \int_{x_1}^{x_p} + \int_{x_p}^{\infty} \right) u^{(\text{s})}(x, y_2) \exp(-i\alpha x) dx. \quad (21)$$

Since $u^{(\text{s})}$ is directly available at $y = y_2$ for $x < x_1$ and $x > x_p$, the first and third integrals above should be transformed into integrals along the complex paths defined by the PML. Accordingly, they become:

$$\begin{aligned}\int_{-\infty}^{x_1} u^{(\text{s})}(x, y_2) \exp(-i\alpha x) dx &= \int_{x_0}^{x_1} u_{\text{PML}}^{(\text{s})}(x, y_2) \exp(-i\alpha \hat{x}) s_x(x) dx, \\ \int_{x_p}^{\infty} u^{(\text{s})}(x, y_2) \exp(-i\alpha x) dx &= \int_{x_p}^{x_{p+1}} u_{\text{PML}}^{(\text{s})}(x, y_2) \exp(-i\alpha \hat{x}) s_x(x) dx,\end{aligned}$$

where $u_{\text{PML}}^{(\text{s})}(x, y_2)$ is the PML-transformed revision of $u^{\text{tot}} - u^{\text{ref}}$. It is denoted as u in Sec. 2, and satisfies Eq. (10).

Since the scattering field $u^{(\text{s})}$ can only propagate upwards for $y > y_2$, we have

$$\hat{u}^{(\text{s})}(\alpha, y) = \hat{u}^{(\text{s})}(\alpha, y_2) \exp(i\beta(y - y_2)).$$

Using the inverse Fourier transform, we obtain the far field for $y > y_2$ as follows

$$u^{(\text{s})}(x, y) = \frac{1}{2\pi} \int_{-\infty}^{\infty} \hat{u}^{(\text{s})}(\alpha, y_2) \exp(i\beta(\alpha)(y - y_2)) \exp(i\alpha x) d\alpha. \quad (22)$$

From the expression $\beta = \sqrt{k_0^2 - \alpha^2}$, we note that β is a pure imaginary number when $\alpha > k_0$; consequently,

Eq. (22) can be rewritten as

$$u^{(s)}(x, y) = \frac{1}{2\pi} \int_{-\alpha}^{\alpha} \hat{u}^{(s)}(\alpha, y_2) \exp(i\beta(\alpha)(y - y_2)) \exp(i\alpha x) d\alpha + \frac{1}{2\pi} \left(\int_{-\infty}^{-\alpha} + \int_{\alpha}^{\infty} \right) \hat{u}^{(s)}(\alpha, y_2) \exp(-\gamma(\alpha)(y - y_2)) \exp(i\alpha x) d\alpha, \quad (23)$$

where $\gamma(\alpha) = \sqrt{\alpha^2 - k_0^2}$ is a non-negative real number. It is obvious that the first and second parts of Eq. (23) are propagating and evanescent waves, respectively. The evanescent wave decays exponentially with the distance $y - y_2$ and therefore does not contribute to the far field.

6 Numerical examples

In this section, we use a phase gradient metasurface [46] shown in Fig. 3 as an example to verify the accuracy and demonstrate the efficiency of our method. It is a 2D metasurface constructed following the approach used in Ref. [47], and it consists of some rectangular cylinders placed on an infinite synthetic sapphire (α -Al₂O₃) slab with refractive index $n_s = 1.7743$ and a thickness of 0.45 μm . These rectangular cylinders are made of Gallium nitride (GaN) with a refractive index $n_c = 2.4431$, a fixed height of 0.5 μm in the y direction and varying widths in the x direction. The refractive indices n_s and n_c correspond to the free space wavelength $\lambda = 0.5 \mu\text{m}$ [48].

The design utilizes 7 distinct cylinder widths given by $0.2(1 - \sqrt{j+6}/4) \mu\text{m}$, $j = 1, 2, \dots, 7$. The metasurface consists of unit cells with a constant size $L = 0.2 \mu\text{m}$ for the x direction. We define $x_j = (j-1)L$ for $j = 1, \dots, p$, then the j -th unit cell occupies the interval (x_j, x_{j+1}) . More specifically, we consider a metasurface with a period of 8 unit cells as shown in Fig. 3, where the first unit cell (x_1, x_2) is an empty one (no cylinder), and the j -th unit cell (x_j, x_{j+1}) contains the cylinder with w_{j-1} for $j = 2, 3, \dots, 8$. Therefore, including the empty cell, there are $p_0 = 8$ distinct unit cells in this device. The scattering problem is for a plane wave with wavelength $\lambda = 2\pi/k_0 = 0.5 \mu\text{m}$ and a zero incident angle illuminating this metasurface from above.

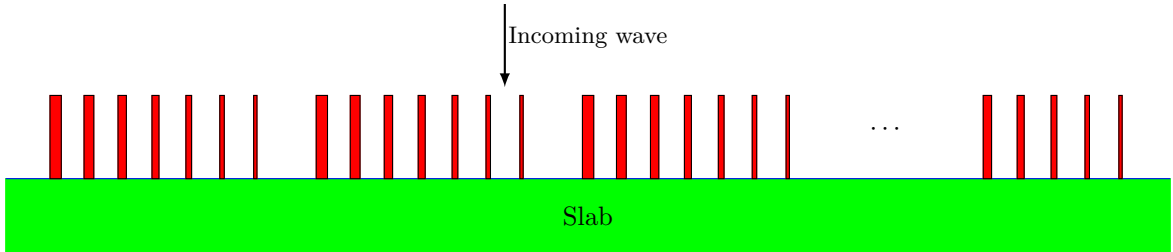


Figure 3: A sketch of 2D phase gradient metasurface.

To validate our method, we first consider a small metasurface with only 7 cylinders. The computational domain contains 9 unit cells where the first and last ones, i.e. (x_1, x_2) and (x_9, x_{10}) , are empty cells. The thicknesses of the left and right PML regions are 0.2 μm . This implies that $p = 10$, $x_0 = -0.2 \mu\text{m}$ and $x_{11} = 2 \mu\text{m}$. In the y direction, we truncate this structure as shown in Fig. 1, and choose $(y_0, y_1, y_{\text{sb}}, y_{\text{st}}, y_2, y_3) = (-0.2, 0, 0.6, 1.05, 2.1, 2.3) \mu\text{m}$. For the PML regions, the positive constant b is around $5.35 \cdot 10^5$. We use our method and the classical FEM to simulate this device, and then compare the results and calculate the relative error of the scattering field $u^{(s)} = u^{\text{tot}} - u^{\text{ref}}$ on the line $y = y_2$ for $x_1 < x < x_p$. The relative error Δ is defined as $\|u_{\text{NtD}}^{(s)}(x, y_2) - u_{\text{FEM}}^{(s)}(x, y_2)\|/\|u_{\text{FEM}}^{(s)}(x, y_2)\|$, where the norm is $\|u\|^2 = \int_{x_1}^{x_p} |u|^2 dx$. For our method, we choose the number of basis functions on different edges as $N_1 = 35$, $N_0 = N_2 = 8$, and $M_j = 15$ ($j = 1, 2, \dots, 9$). The two positive constants in basis functions $\varphi_{k,m}(y)$ are chosen as $C_k^{\varphi} = 5$ ($k = 0, 2$). As a well-tested numerical method, FEM is used for solving the scattering problem in the rectangular domain $(x_0, x_p) \times (y_0, y_3)$ with the same PML parameters. The same reference mesh size h is used for both FEM and our method. It guarantees that the area of every triangular element is bounded by $h^2/2$.

We perform simulations at multiple mesh sizes $h = L/10$, $L/20$, $L/40$ and $L/80$ for both methods. The results are summarized in Tab. 1. For $h = L/10$, our method gives rise to 1966, 1801, 160 and 167 discretization points in Ω_0 , Ω_p , $\Omega_j^{(0)}$ and $\Omega_j^{(2)}$, respectively. For the subdomain $\Omega_j^{(1)}$ ($1 \leq j < p$), the number of points ranges from 1681 to 1723, resulting in a total of 19961 points. For the same mesh size $h = L/10$, FEM yields 22028 discretization points. The corresponding relative error is $\Delta_{L/10} \approx 0.054875$. The data indicates that the relative

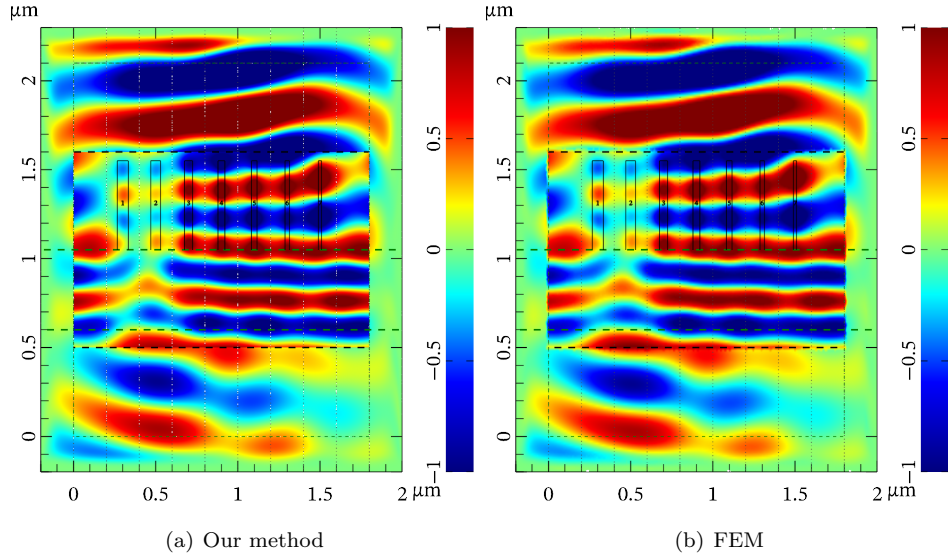


Figure 5: Simulations for the phase gradient metasurface solved by our method (Left) and FEM (Right).

error Δ on a mesh of size h is approximately a quarter of that on a coarser mesh of size $2h$. This shows that the solution obtained by our method converges to the FEM benchmark at a second-order rate, as quantified by $\log_2(\Delta_{2h}/\Delta_h)$. Since FEM with linear elements is of second order accuracy, this result confirms that our method also achieves second-order accuracy.

Table 1: The information of meshes and relative errors

h	Ω_0	Ω_p	$\Omega_j^{(0)}$	$\Omega_j^{(1)}$	$\Omega_j^{(2)}$	Total	FEM	Error Δ	Rate
$L/10$	1966	1801	160	[1681, 1723]	167	19961	22028	0.054875	-
$L/20$	7602	7295	643	[6464, 6528]	643	77218	87506	0.014105	1.96
$L/40$	30177	29379	2461	[25386, 25523]	2456	302454	349131	0.003431	2.04
$L/80$	119735	118230	9586	[100500, 100753]	9592	1196214	1393938	0.000869	1.98

We compare the scattering fields computed by both methods along the line $y = y_2$ for $x_1 < x < x_p$ in Fig. 4. Figure 5 presents the full numerical solution obtained with the reference mesh size $h = L/80$. It displays the total field u^{tot} within the rectangular domain $(0, 1.8) \times (0.5, 1.6)$ μm and the scattered field $u^{(s)}$ in the surrounding region.

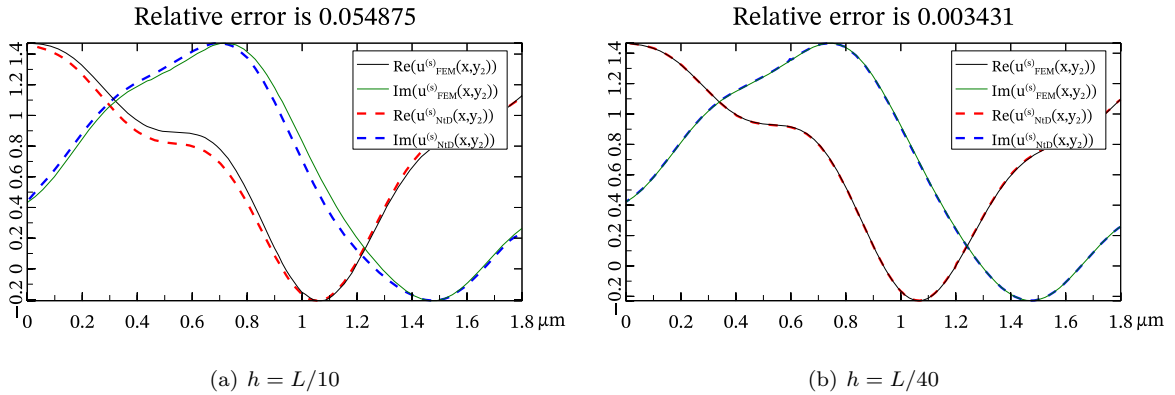


Figure 4: Relative errors of the numerical solutions obtained by our method and FEM.

Next, to demonstrate the efficiency of our method, we simulate the metasurface with a much larger number

of cells by both FEM and our method. From the previous section, it is clear that the NtD matrices can be calculated independently. We develop two separate implementations for our method which calculate the NtD matrices serially and in parallel, respectively. The numerical results are obtained for reference mesh size $h = L/20$. To have a fair comparison, we have calculated the solution on the entire computational domain for both methods. Details of the mesh used in our method are given in Table 1. For FEM, the number of mesh points is around $7940(p + 1)$. Table 2 summarizes the CPU time and peak memory usage for both methods, along with the corresponding relative error Δ .

Table 2: CPU time and peak memory required by these two methods.

$p - 1$	CPU time (seconds)			Peak memory (GB)			Δ
	FEM	Serial NtD	Parallel NtD	FEM	Serial NtD	Parallel NtD	
10	8.52	171.25	28.86	0.7427	0.2430	0.5068	0.013788
100	82.2	171.72	29.42	5.5103	0.2433	0.4560	0.013474
200	169.79	175.01	29.95	10.9329	0.2546	0.4751	0.013730
300	265.39	173.4	30.59	15.9908	0.2643	0.4582	0.013707
400	361.39	173.31	32.42	21.7391	0.2610	0.4629	0.013637
1000	/	176.21	34.08	/	0.3222	0.5317	/
10000	/	222.66	79.85	/	1.6891	1.8945	/
50000	/	438.68	296.6	/	7.7555	7.9761	/
100000	/	732.51	593.75	/	15.3538	15.5836	/
150000	/	1087.90	947.92	/	22.9183	23.0845	/

As discussed in the previous section, our method first computes all NtD matrices, then calculates the normal derivatives of the wave field on the interfaces, and finally recovers the wave field within all subdomains. The computation of NtD matrices is only related to p_0 , N_k ($k = 0, 1, 2$), M_j ($1 \leq j < p$), and the mesh size h . Table 2 indicates that the NtD matrices can be computed in parallel, achieving a speedup of about 6 on a personal computer with an 8-core CPU. Moreover, the CPU time of the second and third steps and peak memory consumption grow at a much slower rate than those of a full domain FEM. The parallel version of our method consumes significantly less CPU time (in the step for calculating the NtD matrices) compared to serial implementation, at the cost of only slightly more memory. The relative error does not change significantly with the increase in the number of unit cells. From Tab. 2, it is clear that our method is highly efficient, advantageous and accurate for simulating large 2D metasurfaces. All the numerical experiments are implemented in C++ and performed on a personal computer with an AMD CPU (8-core Ryzen 7 7840HS) and 32GB memory.

7 Conclusion

In this paper, we propose an NtD-based method for simulating 2D non-periodic metasurfaces, which consist of a huge number of subwavelength elements on a slab. The fundamental assumption is that there are only a relatively small number of distinct elements. This method relies on the NtD operators for subdomains of distinct unit cells and the PML regions. They are approximated by matrices and calculated using the FEM and local function expansions. In the first step, we assemble and solve a block tridiagonal linear system for the normal derivative of the wave field on the interfaces between the unit cells. The number of unknowns in this linear system is much less than that in the classical FEM. In the second step, we recover the wave field inside each unit cell and calculate the far-field, if necessary. Numerical examples indicate that our method is accurate and efficient for simulating large 2D metasurfaces with 10^5 or more subwavelength elements.

Acknowledgements

This work was supported by the Research Grants Council of Hong Kong Special Administrative Region, China (CityU 11317622).

References

[1] A. V. Kildishev, A. Boltasseva, and V. M. Shalaev, “Planar photonics with metasurfaces,” *Science*, vol. 339, no. 6125, 2013.

- [2] M. Khorasaninejad and F. Capasso, "Metalenses: Versatile multifunctional photonic components," *Science*, vol. 358, no. 6367, 2017.
- [3] M. L. Brongersma, R. A. Pala, H. Altug, F. Capasso, W. T. Chen, A. Majumdar, and H. A. Atwater, "The second optical metasurface revolution: moving from science to technology," *Nat. Rev. Electr. Eng.*, vol. 2, no. 2, pp. 125–143, 2025.
- [4] N. Yu and F. Capasso, "Flat optics with designer metasurfaces," *Nat. Mater.*, vol. 13, no. 2, pp. 139–150, 2014.
- [5] X. Ni, Z. J. Wong, M. Mrejen, Y. Wang, and X. Zhang, "An ultrathin invisibility skin cloak for visible light," *Science*, vol. 349, no. 6254, pp. 1310–1314, 2015.
- [6] M. Khorasaninejad, W. T. Chen, R. C. Devlin, J. Oh, A. Y. Zhu, and F. Capasso, "Metalenses at visible wavelengths: Diffraction-limited focusing and subwavelength resolution imaging," *Science*, vol. 352, no. 6290, pp. 1190–1194, 2016.
- [7] T. Santiago-Cruz, S. D. Gennaro, O. Mitrofanov, S. Addamane, J. Reno, I. Brener, and M. V. Chekhova, "Resonant metasurfaces for generating complex quantum states," *Science*, vol. 377, no. 6609, pp. 991–995, 2022.
- [8] G. Soma, K. Komatsu, Y. Nakano, and T. Tanemura, "Complete vectorial optical mode converter using multi-layer metasurface," *Nat. Commun.*, vol. 16, no. 1, 2025.
- [9] S. Gu, C. Mao, A. Guell Izard, S. Sadana, D. Terrel-Perez, M. Mettry-Yassa, W. Choi, W. Zhou, H. Yan, Z. Zhou, T. Massey, A. Abelson, Y. Zhou, S. Huang, C. Daraio, T. U. Tumkur, J. A. Fan, and X. Xia, "3d nanolithography with metalens arrays and spatially adaptive illumination," *Nature*, vol. 648, no. 8094, pp. 591–599, 2025.
- [10] Y. S. Ding and Y. He, "Wave-vector and polarization dependent impedance model for a hexagonal periodic metasurface exemplified through finite-difference time-domain simulations," *Opt. Express*, vol. 25, no. 17, p. 20757, 2017.
- [11] Y. Huang, C. Li, and J. Li, "Developing and analyzing a FDTD method for simulation of metasurfaces," *J. Comput. Appl. Math.*, vol. 460, p. 116364, 2025.
- [12] L. Chen, M. B. Ozakin, R. Zhao, and H. Bagci, "A locally-implicit discontinuous Galerkin time-domain method to simulate metasurfaces using generalized sheet transition conditions," *IEEE Trans. Antennas Propag.*, vol. 71, no. 1, pp. 869–881, 2023.
- [13] C. Li, Y. Huang, and J. Li, "Developing and analyzing a DG method for modeling of metasurfaces," *J. Comput. Phys.*, vol. 534, p. 114011, 2025.
- [14] Y. Vahabzadeh, K. Achouri, and C. Caloz, "Simulation of metasurfaces in finite difference techniques," *IEEE Trans. Antennas Propag.*, vol. 64, no. 11, pp. 4753–4759, 2016.
- [15] S. Sandeep, J.-M. Jin, and C. Caloz, "Finite-element modeling of metasurfaces with generalized sheet transition conditions," *IEEE Trans. Antennas Propag.*, vol. 65, no. 5, pp. 2413–2420, 2017.
- [16] W. Yang, T. Wang, and J. Mao, "Adaptive edge finite element method and numerical design for metasurface cloak," *Comput. Phys. Commun.*, vol. 292, p. 108858, 2023.
- [17] J. Amboli, B. Gallas, G. Demésy, and N. Bonod, "Design and analysis of chiral and achiral metasurfaces with the finite element method," *Opt. Express*, vol. 31, no. 26, p. 43147, 2023.
- [18] J. Mao, W. Wang, and W. Yang, "An adaptive finite element method based on generalized sheet transition conditions and its application to modeling and simulation of functional metasurfaces," *J. Comput. Appl. Math.*, vol. 474, p. 116882, 2026.
- [19] M. A. Francavilla, E. Martini, S. Maci, and G. Vecchi, "On the numerical simulation of metasurfaces with impedance boundary condition integral equations," *IEEE Trans. Antennas Propag.*, vol. 63, no. 5, pp. 2153–2161, 2015.
- [20] G. Cai, X. Liu, T. Shen, J. Liu, N. Liu, and Q. H. Liu, "A full-vectorial spectral element method with generalized sheet transition conditions for high-efficiency metasurface/metafilm simulation," *IEEE Trans. Antennas Propag.*, vol. 71, no. 3, pp. 2652–2660, 2023.

[21] V. Dolean, M. J. Gander, and L. Gerardo-Giorda, “Optimized Schwarz methods for Maxwell’s equations,” *SIAM J. Sci. Comput.*, vol. 31, no. 3, pp. 2193–2213, 2009.

[22] Z. Chen and X. Xiang, “A source transfer domain decomposition method for Helmholtz equations in unbounded domain,” *SIAM J. Numer. Anal.*, vol. 51, no. 4, pp. 2331–2356, 2013.

[23] S. Tao, J. Cheng, and H. Mosallaei, “An integral equation based domain decomposition method for solving large-size substrate-supported aperiodic plasmonic array platforms,” *MRS Commun.*, vol. 6, no. 2, pp. 105–115, 2016.

[24] C. C. Stolk, “A rapidly converging domain decomposition method for the Helmholtz equation,” *J. Comput. Phys.*, vol. 241, pp. 240–252, 2013.

[25] M. J. Gander and H. Zhang, “A class of iterative solvers for the Helmholtz equation: Factorizations, sweeping preconditioners, source transfer, single layer potentials, polarized traces, and optimized Schwarz methods,” *SIAM Rev.*, vol. 61, no. 1, pp. 3–76, 2019.

[26] W. Leng and L. Ju, “An additive overlapping domain decomposition method for the Helmholtz equation,” *SIAM J. Sci. Comput.*, vol. 41, no. 2, pp. A1252–A1277, 2019.

[27] H.-W. Gao, X.-M. Xin, Q. J. Lim, S. Wang, and Z. Peng, “Efficient full-wave simulation of large-scale metasurfaces and metamaterials,” *IEEE Trans. Antennas Propag.*, vol. 72, no. 1, pp. 800–811, 2024.

[28] J. Liu, G. Cai, J. Yao, N. Liu, and Q. H. Liu, “Spectral numerical mode matching method for metasurfaces,” *IEEE Trans. Microwave Theory Tech.*, vol. 67, no. 7, pp. 2629–2639, 2019.

[29] J. Liu, N. Liu, and Q. H. Liu, “Microscopic modeling of metasurfaces by the mixed finite element numerical mode-matching method,” *IEEE Trans. Microwave Theory Tech.*, vol. 68, no. 2, pp. 469–478, 2020.

[30] N. Zhang and Y. Y. Lu, “Spectral Galerkin mode-matching method for applications in photonics,” *Phys. Rev. E*, vol. 109, no. 5, p. 055303, 2024.

[31] R. E. Christiansen, Z. Lin, C. Roques-Carmes, Y. Salamin, S. E. Kooi, J. D. Joannopoulos, M. Soljačić, and S. G. Johnson, “Fullwave Maxwell inverse design of axisymmetric, tunable, and multi-scale multi-wavelength metalenses,” *Opt. Express*, vol. 28, no. 23, p. 33854, 2020.

[32] W. Xue, H. Zhang, A. Gopal, V. Rokhlin, and O. D. Miller, “Fullwave design of cm-scale cylindrical metasurfaces via fast direct solvers,” *arXiv preprint arXiv:2308.08569*, 2023.

[33] A. F. Oskooi, D. Roundy, M. Ibanescu, P. Bermel, J. Joannopoulos, and S. G. Johnson, “MEEP: A flexible free-software package for electromagnetic simulations by the fdtd method,” *Comput. Phys. Comm.*, vol. 181, no. 3, pp. 687–702, 2010.

[34] C. Warren, A. Giannopoulos, A. Gray, I. Giannakis, A. Patterson, L. Wetter, and A. Hamrah, “A CUDA-based GPU engine for gprMax: Open source FDTD electromagnetic simulation software,” *Comput. Phys. Comm.*, vol. 237, pp. 208–218, 2019.

[35] T. W. Hughes, M. Minkov, V. Liu, Z. Yu, and S. Fan, “A perspective on the pathway toward full wave simulation of large area metalenses,” *Appl. Phys. Lett.*, vol. 119, no. 15, 2021.

[36] S. J. Byrnes, A. Lenef, F. Aieta, and F. Capasso, “Designing large, high-efficiency, high-numerical-aperture, transmissive meta-lenses for visible light,” *Opt. Express*, vol. 24, no. 5, p. 5110, 2016.

[37] W. T. Chen, A. Y. Zhu, V. Sanjeev, M. Khorasaninejad, Z. Shi, E. Lee, and F. Capasso, “A broadband achromatic metalens for focusing and imaging in the visible,” *Nat. Nanotechnol.*, vol. 13, no. 3, pp. 220–226, 2018.

[38] R. Pestourie, C. Pérez-Arancibia, Z. Lin, W. Shin, F. Capasso, and S. G. Johnson, “Inverse design of large-area metasurfaces,” *Opt. Express*, vol. 26, no. 26, p. 33732, 2018.

[39] Z. Lin and S. G. Johnson, “Overlapping domains for topology optimization of large-area metasurfaces,” *Opt. Express*, vol. 27, no. 22, p. 32445, 2019.

[40] Z. Hu and Y. Y. Lu, “Efficient analysis of photonic crystal devices by Dirichlet-to-Neumann maps,” *Opt. Express*, vol. 16, no. 22, p. 17383, 2008.

- [41] W. Lu and Y. Y. Lu, “Waveguide mode solver based on Neumann-to-Dirichlet operators and boundary integral equations,” *J. Comput. Phys.*, vol. 231, no. 4, pp. 1360–1371, 2012.
- [42] J.-P. Berenger, “Three-dimensional perfectly matched layer for the absorption of electromagnetic waves,” *J. Comput. Phys.*, vol. 127, no. 2, pp. 363–379, 1996.
- [43] S. D. Gedney, “An anisotropic perfectly matched layer-absorbing medium for the truncation of FDTD lattices,” *IEEE Trans. Antennas Propag.*, vol. 44, no. 12, pp. 1630–1639, 1996.
- [44] X. Jiang, Z. Sun, L. Sun, and Q. Ma, “An adaptive finite element PML method for Helmholtz equations in periodic heterogeneous media,” *Appl. Math. Comput.*, vol. 43, no. 4, 2024.
- [45] T. Lyche, *Numerical linear algebra and matrix factorizations*. Springer International Publishing, 2020.
- [46] D. Lin, P. Fan, E. Hasman, and M. L. Brongersma, “Dielectric gradient metasurface optical elements,” *Science*, vol. 345, no. 6194, pp. 298–302, 2014.
- [47] M. Lawrence, D. R. Barton, J. Dixon, J.-H. Song, J. van de Groep, M. L. Brongersma, and J. A. Dionne, “High quality factor phase gradient metasurfaces,” *Nat. Nanotechnol.*, vol. 15, no. 11, pp. 956–961, 2020.
- [48] M. N. Polyanskiy, “Refractiveindex.info database of optical constants,” *Scientific Data*, vol. 11, no. 1, 2024.

A Additional steps for boundary relationships

At the end of Sec. 3, we only described the two steps for constructing the NtD operator $\Lambda^{(j)}$ and the inhomogeneous vector $f^{(j)}$ in Eq. (5). Here, we discuss the detail for obtaining Eq. (5) from Eqs. (12) and (13). Using Eq. (16), the equations with right-hand side terms $w_j^{(1,-)}$ and $w_j^{(2,+)}$ in Eqs. (13) can be reformulated as

$$w_j^{(1,+)} - w_j^{(\text{ref},1)} = \Lambda_{31}^{(j,0)} \partial_x u_j^{(0)} + \Lambda_{32}^{(j,0)} \partial_x u_{j+1}^{(0)} + \Lambda_{33}^{(j,0)} (\partial_y w_j^{(1,+)} - \partial_y w_j^{(\text{ref},1)}), \quad (24)$$

$$w_j^{(2,-)} - w_j^{(\text{ref},2)} = \Lambda_{11}^{(j,2)} (\partial_y w_j^{(2,-)} - \partial_y w_j^{(\text{ref},2)}) + \Lambda_{12}^{(j,2)} \partial_x u_j^{(2)} + \Lambda_{13}^{(j,2)} \partial_x u_{j+1}^{(2)}. \quad (25)$$

Substitute the first and fourth members of Eqs. (12) into Eqs. (24) and (25), respectively, we have

$$\Lambda_w \begin{bmatrix} \partial_y w_j^{(2,-)} \\ \partial_y w_j^{(1,+)} \end{bmatrix} = V_1 \begin{bmatrix} \partial_x u_j \\ \partial_x u_{j+1} \end{bmatrix} + \begin{bmatrix} w_j^{(\text{ref},2)} \\ w_j^{(\text{ref},1)} \end{bmatrix} - \begin{bmatrix} \Lambda_{11}^{(j,2)} & \\ & \Lambda_{33}^{(j,0)} \end{bmatrix} \begin{bmatrix} \partial_y w_j^{(\text{ref},2)} \\ \partial_y w_j^{(\text{ref},1)} \end{bmatrix}, \quad (26)$$

where

$$\Lambda_w = \begin{bmatrix} \Lambda_{44}^{(j,1)} - \Lambda_{11}^{(j,2)} & \Lambda_{41}^{(j,1)} \\ \Lambda_{14}^{(j,1)} & \Lambda_{11}^{(j,1)} - \Lambda_{33}^{(j,0)} \end{bmatrix}, \quad u_j = \begin{bmatrix} u_j^{(0)} \\ u_j^{(1)} \\ u_j^{(2)} \end{bmatrix},$$

$$V_1 = \begin{bmatrix} 0 & -\Lambda_{42}^{(j,1)} & \Lambda_{12}^{(j,2)} & 0 & -\Lambda_{43}^{(j,1)} & \Lambda_{13}^{(j,2)} \\ \Lambda_{31}^{(j,0)} & -\Lambda_{12}^{(j,1)} & 0 & \Lambda_{32}^{(j,0)} & -\Lambda_{13}^{(j,1)} & 0 \end{bmatrix}.$$

Let Λ_w^{-1} be the inverse operator of Λ_w , we can solve Eq. (26) for $\partial_y w_j^{(2,-)}$ and $\partial_y w_j^{(1,+)}$ as follows:

$$\begin{bmatrix} \partial_y w_j^{(2,-)} \\ \partial_y w_j^{(1,+)} \end{bmatrix} = \Lambda_w^{-1} V_1 \begin{bmatrix} \partial_x u_j \\ \partial_x u_{j+1} \end{bmatrix} + f_w^{(j)}, \quad (27)$$

where

$$f_w^{(j)} = \Lambda_w^{-1} \begin{bmatrix} w_j^{(\text{ref},2)} \\ w_j^{(\text{ref},1)} \end{bmatrix} - \Lambda_w^{-1} \begin{bmatrix} \Lambda_{11}^{(j,2)} & \\ & \Lambda_{33}^{(j,0)} \end{bmatrix} \begin{bmatrix} \partial_y w_j^{(\text{ref},2)} \\ \partial_y w_j^{(\text{ref},1)} \end{bmatrix}.$$

The equations with right-hand-side terms $u_j^{(k)}$ and $u_{j+1}^{(k)}$ ($j = 0, 1, 2$) in Eqs. (12) and (13) can be written as

$$\begin{bmatrix} u_j \\ u_{j+1} \end{bmatrix} = G^{(j)} \begin{bmatrix} \partial_x u_j \\ \partial_x u_{j+1} \end{bmatrix} + V_3 \begin{bmatrix} \partial_y w_j^{(2,-)} \\ \partial_y w_j^{(1,+)} \end{bmatrix} - V_4 \begin{bmatrix} \partial_y w_j^{(\text{ref},2)} \\ \partial_y w_j^{(\text{ref},1)} \end{bmatrix}, \quad (28)$$

where

$$G^{(j)} = \begin{bmatrix} \Lambda_{11}^{(j,0)} & & & & & \\ & \Lambda_{22}^{(j,1)} & \Lambda_{12}^{(j,0)} & & & \\ & & \Lambda_{22}^{(j,2)} & \Lambda_{23}^{(j,1)} & & \\ \Lambda_{21}^{(j,0)} & & & \Lambda_{23}^{(j,2)} & & \\ & \Lambda_{32}^{(j,1)} & & & \Lambda_{22}^{(j,0)} & \\ & & \Lambda_{32}^{(j,2)} & & & \Lambda_{33}^{(j,1)} \end{bmatrix}, \quad V_3 = \begin{bmatrix} \Lambda_{13}^{(j,0)} \\ \Lambda_{24}^{(j,1)} \\ \Lambda_{21}^{(j,2)} \\ \Lambda_{34}^{(j,2)} \\ \Lambda_{31}^{(j,1)} \\ \Lambda_{31}^{(j,2)} \end{bmatrix}, \quad V_4 = \begin{bmatrix} \Lambda_{13}^{(j,0)} \\ \Lambda_{21}^{(j,2)} \\ \Lambda_{23}^{(j,0)} \\ \Lambda_{31}^{(j,1)} \\ \Lambda_{31}^{(j,2)} \end{bmatrix}.$$

Substitute Eq. (27) into Eq. (28), we have

$$\begin{bmatrix} u_j \\ u_{j+1} \end{bmatrix} = \Lambda^{(j)} \begin{bmatrix} \partial_x u_j \\ \partial_x u_{j+1} \end{bmatrix} + f^{(j)}, \quad \Lambda^{(j)} = G^{(j)} + V_3 A_w^{-1} V_1, \quad f^{(j)} = V_3 f_w^{(j)} - V_4 \begin{bmatrix} \partial_y w_j^{(\text{ref},2)} \\ \partial_y w_j^{(\text{ref},1)} \end{bmatrix}. \quad (29)$$

B Approximation by local function expansion

In Sec. 4, to make the content simple, we simplify the notations of some quantities, such as NtD matrices, approximations for some functions and the related column vectors. Here, we give the following approximations for all functions

$$w_j^{(k,\pm)} \approx \sum_{m=1}^{M_j} \tilde{w}_{j,m}^{(k,\pm)} \phi_{j,m}(x), \quad \partial_y w_j^{(k,\pm)} \approx \sum_{m=1}^{M_j} \partial_y \tilde{w}_{j,m}^{(k,\pm)} \phi_{j,m}(x), \quad x \in (x_j, x_{j+1}), \quad k = 1, 2, \quad (30)$$

$$u_j^{(k)} \approx \sum_{m=1}^{N_k} \tilde{u}_{j,m}^{(k)} \varphi_{k,m}(y), \quad \partial_x u_j^{(k)} \approx \sum_{m=1}^{N_k} \partial_x \tilde{u}_{j,m}^{(k)} \varphi_{k,m}(y), \quad y \in (y_k, y_{k+1}), \quad k = 0, 1, 2, \quad (31)$$

$$w_j^{(\text{ref},k)} \approx \sum_{m=1}^{M_j} \tilde{w}_{j,m}^{(\text{ref},k)} \phi_{j,m}(x), \quad \partial_y w_j^{(\text{ref},k)} \approx \sum_{m=1}^{M_j} \partial_y \tilde{w}_{j,m}^{(\text{ref},k)} \phi_{j,m}(x), \quad x \in (x_j, x_{j+1}), \quad k = 1, 2, \quad (32)$$

$$u_1^{(1)} \approx \sum_{m=1}^{N_1} \tilde{u}_{1,m}^{(\text{ref},1)} \varphi_{1,m}(y), \quad \partial_x u_1^{(\text{ref},1)} \approx \sum_{m=1}^{N_1} \partial_x \tilde{u}_{1,m}^{(\text{ref},1)} \varphi_{1,m}(y), \quad y \in (y_1, y_2). \quad (33)$$

In Eqs. (17) and (18), there are some column vectors (e.g. $\tilde{u}_j^{(1)}$, $\partial_x \tilde{u}_j^{(1)}$), their elements are the expansion coefficients of the corresponding approximations (Eqs. (30) - (33)), we add a subscript m to a vector to denote its m th element. These column vectors are

$$\begin{aligned} \tilde{u}_j^{(k)} &= \left[\tilde{u}_{j,1}^{(k)}, \dots, \tilde{u}_{j,N_k}^{(k)} \right], & \partial_x \tilde{u}_j^{(k)} &= \left[\partial_x \tilde{u}_{j,1}^{(k)}, \dots, \partial_x \tilde{u}_{j,N_k}^{(k)} \right], & 1 \leq j \leq p, \quad k = 0, 1, 2, \\ \tilde{w}_j^{(k,\pm)} &= \left[\tilde{w}_{j,1}^{(k,\pm)}, \dots, \tilde{w}_{j,M_j}^{(k,\pm)} \right], & \partial_y \tilde{w}_j^{(k,\pm)} &= \left[\partial_y \tilde{w}_{j,1}^{(k,\pm)}, \dots, \partial_y \tilde{w}_{j,M_j}^{(k,\pm)} \right], & 1 \leq j < p, \quad k = 1, 2, \\ \tilde{u}_j^{(\text{ref},1)} &= \left[\tilde{u}_{j,1}^{(\text{ref},1)}, \dots, \tilde{u}_{j,N_1}^{(\text{ref},1)} \right], & \partial_x \tilde{u}_j^{(\text{ref},1)} &= \left[\partial_x \tilde{u}_{j,1}^{(\text{ref},1)}, \dots, \partial_x \tilde{u}_{j,N_1}^{(\text{ref},1)} \right], & j = 1, p, \\ \tilde{w}_j^{(\text{ref},k)} &= \left[\tilde{w}_{j,1}^{(\text{ref},k)}, \dots, \tilde{w}_{j,M_j}^{(\text{ref},k)} \right], & \partial_y \tilde{w}_j^{(\text{ref},k)} &= \left[\partial_y \tilde{w}_{j,1}^{(\text{ref},k)}, \dots, \partial_y \tilde{w}_{j,M_j}^{(\text{ref},k)} \right], & 1 \leq j < p. \end{aligned}$$